

Atmospheric Circulation Trends, 1950–2000: The Relative Roles of Sea Surface Temperature Forcing and Direct Atmospheric Radiative Forcing

CLARA DESER AND ADAM S. PHILLIPS

Climate and Global Dynamics Division, National Center for Atmospheric Research, Boulder, Colorado*

(Manuscript received 30 January 2008, in final form 30 June 2008)

ABSTRACT

The relative roles of direct atmospheric radiative forcing (due to observed changes in well-mixed greenhouse gases, tropospheric and stratospheric ozone, sulfate and volcanic aerosols, and solar output) and observed sea surface temperature (SST) forcing of global December–February atmospheric circulation trends during the second half of the twentieth century are investigated by means of experiments with an atmospheric general circulation model, Community Atmospheric Model, version 3 (CAM3). The model experiments are conducted by specifying the observed time-varying SSTs and atmospheric radiative quantities individually and in combination. This approach allows the authors to isolate the direct impact of each type of forcing agent as well as to evaluate their combined effect and the degree to which their impacts are additive. CAM3 realistically simulates the global patterns of sea level pressure and 500-hPa geopotential height trends when both forcings are specified. SST forcing and direct atmospheric radiative forcing drive distinctive circulation responses that contribute about equally to the global pattern of circulation trends. These distinctive circulation responses are approximately additive and partially offsetting. Atmospheric radiative changes directly drive the strengthening and poleward shift of the midlatitude westerly winds in the Southern Hemisphere (and to a lesser extent may contribute to those over the Atlantic–Eurasian sector in the Northern Hemisphere), whereas SST trends (specifically those in the tropics) are responsible for the intensification of the Aleutian low and weakening of the tropical Walker circulation. Discrepancies between the atmospheric circulation trends simulated by CAM3 and Community Climate System Model, version 3 (CCSM3), a coupled model driven by the same atmospheric radiative forcing as CAM3, are traced to differences in their tropical SST trends: in particular, a 60% weaker warming of the tropical Indo-Pacific in the CCSM3 ensemble mean than in nature.

1. Introduction

The atmospheric circulation plays a central role in climate, influencing the global distributions of precipitation and air temperature. Since the middle of the twentieth century, the large-scale circulation has exhibited numerous changes, including an intensification of the midlatitude westerlies over the North Pacific, North Atlantic, and Southern Oceans, and a weakening of the trade winds over the tropical Pacific (Trenberth and Hurrell 1994; Hurrell 1995; Clarke and Lebedev 1996;

Hines et al. 2000; Thompson et al. 2000; Marshall 2003; Tanaka et al. 2004; Power and Smith 2007). These circulation trends have contributed to coherent patterns of precipitation and temperature anomalies worldwide (Hurrell 1996; Hurrell and van Loon 1997; Deser et al. 2004; Hegerl and Kenyon 2008).

The causes of observed atmospheric circulation trends over the last half century are a subject of ongoing investigation. Greenhouse gas concentration increases and stratospheric ozone depletion are considered to be the main factors responsible for the intensification of the westerlies over the Southern Ocean (Stephenson and Held 1993; Fyfe et al. 1999; Kushner et al. 2001; Thompson and Solomon 2002; Arblaster and Meehl 2006; Gillett and Thompson 2003; Thompson and Solomon 2005; Cai and Cowan 2007; Hegerl et al. 2007), while tropical sea surface temperature (SST) changes are implicated in the circulation trends over the North Pacific (Graham 1994; Trenberth and Hurrell

* The National Center for Atmospheric Research is sponsored by the National Science Foundation.

Corresponding author address: Dr. Clara Deser, Climate and Global Dynamics Division, NCAR, P.O. Box 3000, Boulder, CO 80307.
E-mail: cdeser@ucar.edu

1994; Deser et al. 2004). The latter may also play a contributing role to circulation trends over the North Atlantic (Hoerling et al. 2004; Hurrell et al. 2004), although intrinsic variability due to nonlinear atmospheric dynamics is also important (Schneider et al. 2003; Hurrell et al. 2004; Bracco et al. 2004). Thus, there is evidence that both SST changes and atmospheric radiative forcing due to changes in greenhouse gas and ozone concentrations have contributed to atmospheric circulation trends in recent decades. Note, however, that the two forcing agents are not necessarily independent, since SSTs also respond to changes in atmospheric radiative forcing.

Global coupled climate models can be insightful for understanding the atmospheric circulation response to increasing greenhouse gas concentrations, since they contain both the direct effects of atmospheric radiative forcing (via differential changes in atmospheric heating) and the indirect effects (via changes in SST). However, for the purpose of attribution in the real climate system, they also have inherent limitations, since their SST response (and especially the regional details of their SST response) may differ from the observed SST evolution, thereby affecting the fidelity of the simulated circulation trends (Gillett et al. 2005; Hegerl et al. 2007).

One way to circumvent this limitation is to specify the observed time-evolving distribution of SSTs and atmospheric radiative forcing in an atmosphere-only model. While this approach does not address the origin (natural or anthropogenic) of the SST changes, it does ensure that the oceanic forcing is realistic. We note that there is a long history of atmospheric model integrations driven by observed time-varying SSTs as the lower boundary condition, the so-called Atmospheric Model Intercomparison Project (AMIP) configuration (Gates et al. 1999). These traditional AMIP experiments do not, however, take into account the direct effects of atmospheric radiative forcing upon the circulation.

The methodology of specifying both the observed time-evolving distributions of SST and atmospheric radiative forcing in an atmosphere-only model was first introduced by Folland et al. (1998). Note that this approach does not “double count” the atmospheric radiative forcing because only the direct effect is specified, whereas the indirect effect is included in the prescribed SST forcing. Folland et al. (1998) focused on the vertical structure of the temperature trend response in the troposphere and lower stratosphere during 1961–94 to SST versus direct atmospheric radiative forcing. Using a similar methodology, Compo and Sardeshmukh (2008) found that the recent warming over land has

occurred as a response to oceanic warming through enhanced downward longwave radiation due to increased atmospheric moisture rather than as a direct response to increasing greenhouse gases.

Following the same approach, Bracco et al. (2004) investigated the atmospheric circulation response to observed SST forcing versus direct atmospheric radiative forcing over the second half of the twentieth century using an atmospheric GCM of intermediate complexity and idealized atmospheric radiative forcing. Focusing on the response of the extratropical Northern Hemisphere circulation during winter, they found that SST variations contributed to trends over the Pacific–North American sector with a partially counteracting effect from greenhouse gas increases, while trends over the North Atlantic–European region are primarily consistent with intrinsic variability and a weak (and not statistically significant) contribution from greenhouse gas increases.

The same methodology has been used for understanding future projections of atmospheric circulation change. In particular, Cash et al. (2005) found that the circulation response of an atmospheric general circulation model (AGCM) to combined forcing from doubled CO₂ and tropical SST changes at the time of CO₂ doubling is consistent with the circulation response to doubled CO₂ in a coupled ocean–atmosphere GCM from which the SST changes were taken. Cash et al. (2005) did not investigate the individual impacts of CO₂ and tropical SST anomalies upon the model’s atmospheric circulation. This issue was addressed in an earlier study by Stephenson and Held (1993), who found that the winter stationary wave response over the North Pacific and Canada as well as the increase in the Southern Hemisphere westerlies in a doubled CO₂ scenario was due to SST forcing rather than direct atmospheric radiative forcing.

In this study, we analyze the relative roles of SST and atmospheric radiative changes in forcing global atmospheric circulation trends during 1950–2000 by means of ensemble simulations with Community Atmospheric Model, version 3 (CAM3). The atmospheric radiative forcing includes changes in greenhouse gases, tropospheric and stratospheric ozone, sulfate and volcanic aerosols, and solar output, taken from Meehl et al. (2003). The CAM3 experiments are conducted by specifying the observed time-varying SSTs and atmospheric radiative quantities individually and in combination. This approach allows us to isolate the direct impact of each type of forcing agent, as well as to evaluate their combined effect and the degree to which their impacts are additive. We also assess the role of tropical SST variations by means of additional CAM3 integra-

tions, and compare the simulated atmospheric circulation trends in CAM3 with those in the coupled Community Climate System Model, version 3 (CCSM3, of which CAM3 is the atmospheric component model) over the same time period. It is important to note that this study does not attempt to distinguish anthropogenic from natural forcing of recent atmospheric circulation trends; rather, it assesses the relative roles of oceanic and direct atmospheric radiative driving. However, we draw some possible inferences regarding the role of anthropogenic forcing from the comparison between the CAM3 and CCSM3 results.

There are shortcomings to the design and physical interpretation of all atmosphere-only model experiments because of the lack of coupling with an underlying ocean. In particular, traditional AMIP experiments have been criticized for specifying SST variations in regions where these are due to, and not a cause of, overlying atmospheric circulation changes (e.g., Kumar and Hoerling 1998; Bretherton and Battisti 2000). This is particularly an issue in the extratropics where the dominant direction of interaction is that of the atmosphere forcing the ocean (e.g., Cayan 1992; Deser and Timlin 1997) and may also be a factor in certain portions of the tropics, for example the Indian Ocean (Kumar and Hoerling 1998; Klein et al. 1999; Deser and Phillips 2006); it is less of a concern in the tropical Pacific where SST anomalies are known to exert a direct effect on deep atmospheric convection. As we shall show, the atmospheric circulation trends simulated by CAM3 in response to SST forcing are largely a result of SST changes in the tropics, and in particular, rainfall changes over the equatorial Pacific. Thus, we do not consider the AMIP experimental design to be unduly problematic in our case, although it remains a caveat in the interpretation of our results. By the same token, atmosphere-only model experiments forced with changes in greenhouse gas concentrations and other radiatively important chemical constituents contain artificially large downward surface energy fluxes because of the lack of an interactive ocean. Nevertheless, atmosphere-only model experiments remain a useful albeit imperfect tool for probing the physical mechanisms of the atmospheric circulation response to different types of forcing.

In this study, we examine the global atmospheric circulation trends during 1950–2000 and address the following questions. How realistic are the trends simulated by CAM3 when forced with the combined observed evolution of SST forcing and atmospheric radiative forcing? Which components of the simulated trends are due to SST and which to direct atmospheric radiative forcing, and how are they related? To what

extent are the responses to the two types of forcing additive? How do the trends in the CAM3 simulations compare with those in CCSM3, and what is the origin of their differences? We focus on the boreal winter season, December–February (DJF), when the simulated circulation trends are most similar to their observed counterparts. Model simulations are not available past the year 2000, precluding any analysis of trends extending into the twenty-first century.

The rest of the paper is organized as follows. The model simulations, observational datasets, and methodology are described in section 2. The results are presented in section 3. A summary and discussion are provided in section 4.

2. Data and methods

a. Model and observational datasets

The primary model archive for this study is a set of simulations conducted with CAM3 at two horizontal resolutions: T85, equivalent to 1.4° latitude \times 1.4° longitude; and T42, equivalent to 2.8° latitude \times 2.8° longitude. The physical and numerical methods used in CAM3 are given in Collins et al. (2006) and references therein. The model's mean state and interannual variability are described in Hurrell et al. (2006), Hack et al. (2006), and Deser et al. (2006).

Four sets of ensemble integrations were performed with CAM3, labeled according to their forcing characteristics (see Table 1). The “SST+ATM” ensemble is forced by the observed evolution of global SSTs and sea ice concentrations plus atmospheric chemical composition (greenhouse gases, tropospheric and stratospheric ozone, and sulfate and volcanic aerosols) and solar output during 1950–2000. The “SST” ensemble is forced by the observed evolution of global SSTs and sea ice concentrations during 1950–2000, with atmospheric chemical composition and solar output set at 1990 levels. The “Tropical SST” ensemble is identical to the SST ensemble except that SSTs poleward of 20°N and poleward of 20°S are set to their climatological mean seasonal cycles. The ATM ensemble is forced by the observed evolution of atmospheric chemical composition and solar output during 1950–2000 (identical to that in SST+ATM), with SSTs and sea ice concentrations set to their climatological mean seasonal cycles.

The SST and sea ice concentrations are from the dataset of Hurrell et al. (2008), and the atmospheric forcing fields are given in Meehl et al. (2006) and are identical to those used for the twentieth-century integrations of CCSM3. The SST+ATM, SST and Tropical SST ensembles each consist of 5 integrations at T85 resolution and 5 integrations at T42 resolution. Given

TABLE 1. The forcing characteristics, horizontal resolution, and ensemble size of the CAM3 integrations used in this study.

Forcing characteristics		Horizontal resolution	Ensemble size
SST+ATM	Observed evolution of global SSTs, sea ice concentrations, atmospheric chemical composition, and solar output during 1950–2000	T42	5
		T85	5
SST	Observed evolution of global SSTs and sea ice concentrations during 1950–2000; atmospheric chemical composition and solar output fixed at 1990 levels	T42	5
		T85	5
Tropical SST	Observed evolution of tropical (20°N–20°S) SSTs during 1950–2000; SSTs elsewhere and sea ice concentrations set to their climatological seasonal cycles; atmospheric chemical composition and solar output fixed at 1990 levels	T42	5
		T85	5
ATM	Observed evolution of atmospheric chemical composition and solar output during 1950–2000; global SSTs and sea ice concentrations set to their climatological seasonal cycles	T42	10

the similarity between the ensemble mean atmospheric circulation trends at T42 and T85 (not shown), we have averaged the trends from the two model resolutions together to form 10-member ensemble means. The ATM ensemble consists of 10 integrations at T42 resolution.

In addition to the atmosphere-only model integrations, we analyze a 7-member ensemble of twentieth-century (1870–1999) simulations with CCSM3 (Collins et al. 2006), a global coupled climate model run without flux adjustments. CCSM3 is composed of an atmospheric model (CAM3), an ocean model (the Parallel Ocean Program), a land model (the Community Land Model), and a sea ice model (the Community Sea Ice Model version 4). The CCSM3 simulations are conducted at T85 horizontal resolution and forced with the same evolution of atmospheric chemical composition and solar output as the SST+ATM and ATM experiments. The evolution of global mean air and ocean temperatures over the twentieth century from the CCSM3 simulations are documented in Meehl et al. (2006).

We make use of several observational datasets, including: sea level pressure (SLP) from the International Comprehensive Ocean–Atmosphere Dataset (ICOADS; Worley et al. 2005) on a 2° latitude × 2° longitude grid; SLP from the Hadley Centre’s Mean Sea Level Pressure Dataset (HadSLP2; Allan and Ansell 2006) on a 5° latitude × 5° longitude grid; and SLP and 500-hPa geopotential heights (Z500) from the National Centers for Environmental Prediction–National Center for Atmospheric Research (NCEP–NCAR) 40-Year (50-Year) Reanalysis Project (Kalnay et al. 1996; Kistler et al. 2001) on a 2.5° latitude × 2.5° longitude grid. These observational archives differ in their spatial coverage as well as in their degree and sophistication of data processing: ICOADS is an archive of surface marine observations containing minimal data processing (e.g., standard quality control procedures but

no filling in of missing data); HadSLP2 is an optimally interpolated blended archive of land station records and marine observations from the ICOADS; and the NCEP–NCAR 40-Year (50-Year) Reanalysis Project is a state-of-the-art model–data assimilation system. For the data-sparse high-latitude region of the Southern Hemisphere, we use station-based SLP indices of the southern annular mode (SAM) from an updated version of Marshall (2003).

b. Methods

We use linear trend analysis as a simple way of characterizing changes in atmospheric circulation that have occurred over the period of study as a whole (1950–2000). This approach is validated using epoch difference analysis [(1981–2000) – (1950–61)], which yields practically identical results (not shown). To compute the linear trends, we first formed monthly anomalies by subtracting the long-term monthly means based on the period 1950–2000 from each calendar month. The monthly anomalies were then averaged over the boreal winter season (DJF), and the DJF trends computed using least squares linear regression. The statistical significance of the linear trend values was assessed by means of a 2-sided Student’s *t* test taking into account serial correlation (von Storch and Zwiers 1999). Thus, the statistical significances of the trend values are evaluated with respect to interannual variability.

For the ICOADS, which contains substantial amounts of missing data, a trend was computed only if at least 25% of the winters in a given grid box had data. To improve the readability of the trend maps based on the ICOADS, linear interpolation (across gaps not exceeding 5 points in longitude and 3 points in latitude) and weighted binomial smoothing (9 points in longitude and 3 points in latitude) were applied to the trend values.

SLP Linear Trend, DJF 1950-2000

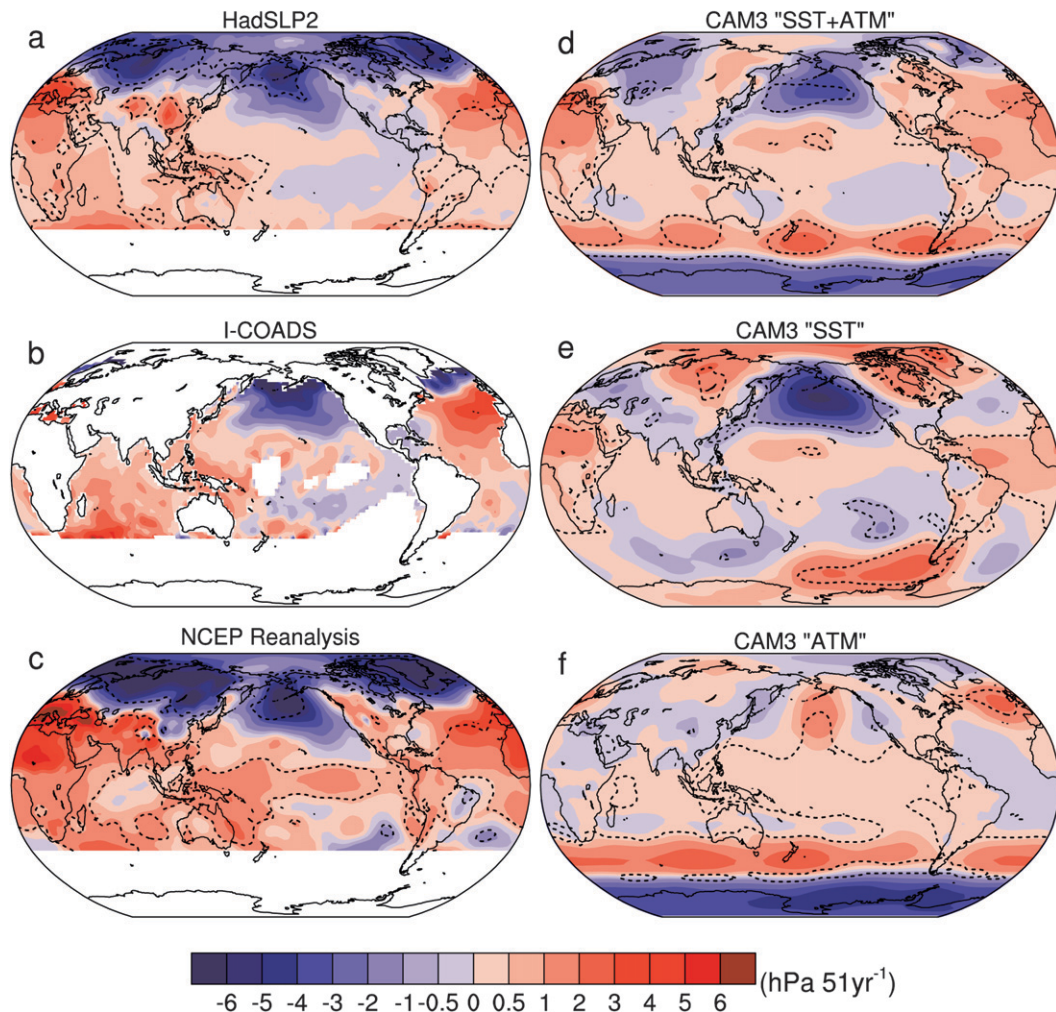


FIG. 1. Linear trends [color shading; $\text{hPa} (51 \text{ yr})^{-1}$] of DJF SLP during 1950–2000 from (left) observations and (right) CAM3 model simulations. Results are shown for 3 observational datasets: (a) HadSLP2, (b) ICOADS, and (c) NCEP–NCAR reanalyses; and 3 sets of CAM3 model simulations: (d) SST+ATM, (e) SST, and (f) ATM. Values south of 40°S are omitted in the left-hand panels because of a lack of reliable observations dating back to 1950. Dashed contours indicate trends that are significantly different from zero at the 95% level.

3. Results

a. SST+ATM versus observations

Observed DJF SLP trends from 1950 to 2000 are shown in Fig. 1 (left) based on three different datasets (HadSLP2, ICOADS, and NCEP–NCAR reanalyses). Values south of 40°S are omitted because of a lack of reliable observations dating back to 1950 (Hines et al. 2000; Marshall 2003). The three observational datasets agree on the overall pattern of SLP trends: negative values over high latitudes of the Northern Hemisphere and the North Pacific and positive values over midlatitudes of the Northern Hemisphere except the Pacific sector (maxi-

imum amplitudes approximately $4\text{--}6 \text{ hPa} (51 \text{ yr})^{-1}$, and weaker trends over the tropics (negative values over the eastern tropical Pacific and positive values elsewhere). The trends in the NCEP–NCAR reanalyses are larger than those in either the ICOADS or HadSLP2. Regionally, the largest trends occur over the North Pacific, North Atlantic, Eurasia, and northern Africa: all are significantly different from zero at the 95% level. The negative trend over the North Pacific is indicative of a deepening of the Aleutian low, while over the Atlantic–Eurasian sector the negative trend over high latitudes coupled with the positive trend over midlatitudes is indicative of a positive trend in the North Atlantic Oscillation (NAO; Hurrell 1995).

The pattern of SLP trends simulated in the SST+ATM ensemble mean (Fig. 1d) compares well with observations: the pattern correlation is 0.73 with HadSLP2 and 0.65 with NCEP–NCAR reanalyses based on area-weighted anomalies north of 40°S. In particular, the model simulates the deepening trend of the Aleutian low, the positive trend in the NAO (although not statistically significant as it is in observations), and the pattern of trends over the tropics (especially when compared with the HadSLP2 dataset). The magnitudes of the simulated SLP trends are generally smaller than observed over the Northern Hemisphere extratropics, while they are comparable to the HadSLP2 and ICOADS observations but weaker than the NCEP–NCAR reanalyses over the tropics.

In the Southern Hemisphere, the SST+ATM ensemble mean simulates a zonally symmetric pattern of positive SLP trends in midlatitudes (35°–55°S) and negative trends at high latitudes (south of 55°S), indicative of a positive trend in the SAM (Thompson et al. 2000; Marshall 2003). Although the gridded observational datasets are unreliable for computing SLP trends south of 40°S before the 1970s (see Arblaster and Meehl 2006), a dozen station records may be used to define the SAM back to 1957 (Marshall 2003). Six stations are located within the midlatitude (37°–47°S) center of action of the SAM and six within the high-latitude center of action (65°–71°S). The observed SLP trends for the mid- and high-latitude centers of action during the period 1957–2000 are 1.6 hPa (44 yr)^{−1} and −2.5 hPa (44 yr)^{−1}, respectively; statistically significant at the 95% confidence level. The simulated trends in the SST+ATM ensemble mean are in good agreement with the station-based observational estimates, with values of 1.4 hPa (44 yr)^{−1} and −3.6 hPa (44 yr)^{−1} for the mid- and high-latitude centers of action, respectively, based on zonally averaged SLP anomalies during the period 1957–2000 (significant at the 95% confidence level). We defer discussion of the SLP trends simulated in the SST and ATM ensemble means (Figs. 1d,f) to section 3b.

The observed trends in Z500 from the NCEP–NCAR reanalyses are shown in Fig. 2a (as for SLP, values south of 40°S are omitted because of a lack of reliable data). In the extratropics, the pattern of Z500 trends is similar to that of SLP, consistent with the equivalent barotropic structure of the annular modes and the Aleutian low, which is associated with the Pacific–North American (PNA) pattern in the middle and upper troposphere (Trenberth and Hurrell 1994). In the tropics, the trends in Z500 [and (Z1000 − Z500) thickness; not shown] are positive everywhere, reflecting a general warming of the lower troposphere. The pattern of Z500 trends simu-

Z500 Linear Trend, DJF 1950–2000

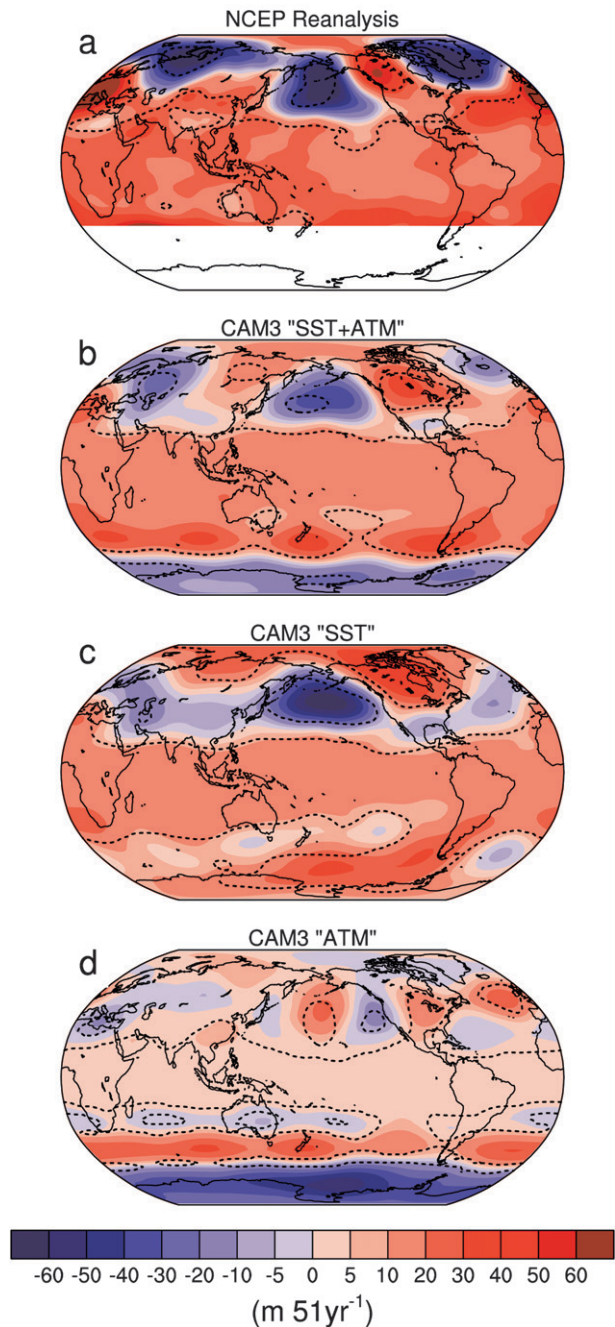


FIG. 2. Same as in Fig. 1, but for 500-hPa geopotential height [Z_{500} ; m (51 yr)^{-1}]. (a) NCEP–NCAR reanalyses, (b) SST+ATM, (c) SST, and (d) ATM.

lated by the SST+ATM ensemble mean (Fig. 2b) compares well with observations: the pattern correlation is 0.76 with the NCEP–NCAR reanalyses based on area-weighted anomalies north of 40°S. Like SLP, the Z500 trend magnitudes are underestimated in the

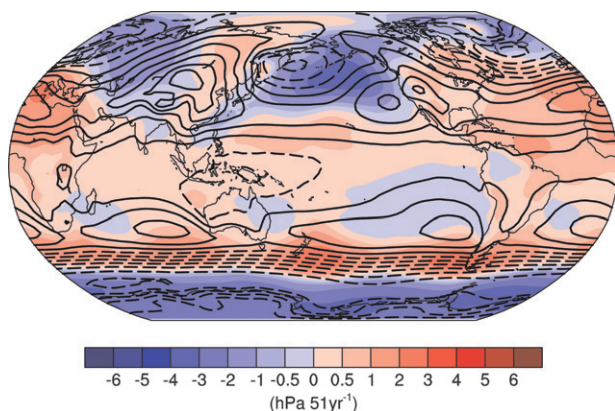


FIG. 3. Linear trends of DJF SLP during 1950–2000 (color shading) superimposed upon the climatological mean SLP distribution (contours) from the CAM3 SST+ATM ensemble mean. The climatology is contoured every 4 hPa, with dashed contours for values ≤ 1008 hPa.

model ensemble mean compared to the NCEP–NCAR reanalyses.

To provide a context for the circulation changes, the simulated SLP trend (color shading) is superimposed upon the climatological mean SLP distribution (contours) from the SST+ATM ensemble mean in Fig. 3. The negative SLP trend over the North Pacific reflects a deepening and eastward extension of the Aleutian low, and a weakening of the subtropical high off the coast of California. The negative (positive) SLP trend over the northern (central) North Atlantic extending eastward over Europe and North Africa reflect an in situ strengthening and a slight northward shift of the mean Icelandic low and Azores high. In contrast, in the Southern Hemisphere, positive SLP trends are located along the southern flanks of the subtropical highs within the zone of maximum mean meridional SLP gradient. Coupled with negative SLP trends over the mean polar low, this trend pattern is indicative of a poleward shift and intensification of the Southern Hemisphere midlatitude westerlies. In the tropics, the SLP trends are indicative of a weakening of the mean zonal pressure gradient across the Indo-Pacific (e.g., a weakening of the Walker circulation). Similar relationships between the trend and climatology are found for Z500 from the model simulations and for SLP and Z500 from observations (not shown).

To give an idea of the sampling distribution of the simulated trend patterns in the SST+ATM ensemble, histograms of the trend pattern correlations between each ensemble member and the ensemble mean are shown in Figs. 4a,b for SLP and Z500, respectively. Out of 10 ensemble members, 9 exhibit pattern correlations with the ensemble mean that exceed 0.6 (0.7) for SLP

(Z500). Analogous histograms of the pattern correlations for each of the 10 SST+ATM ensemble members with observations (HadSLP2 for SLP and NCEP–NCAR reanalysis for Z500) exhibit a larger spread than those with the model's ensemble mean, but the majority (70%–80%) of ensemble members exhibit pattern correlations exceeding 0.5 (Figs. 4c,d). The highest pattern correlation between a single ensemble member and observations is 0.76 for SLP and 0.79 for Z500, and the lowest is -0.26 for SLP and 0.20 for Z500.

b. SST forcing versus direct atmospheric radiative forcing

Given the overall agreement between the observed and simulated SST+ATM ensemble mean trend patterns for both SLP and Z500, we proceed to examine the relative contributions of SST forcing and direct atmospheric radiative forcing in driving the simulated trends (Figs. 1e,f and 2c,d). It is evident that the different forcing agents produce distinctive spatial patterns of atmospheric circulation response. Direct atmospheric radiative forcing is responsible for the zonally symmetric circulation response over the Southern Hemisphere extratropics (e.g., the positive trend in the SAM) and to a lesser extent the positive trend in the NAO, although the centers of action are northward-shifted with respect to the canonical pattern. Sea surface temperature forcing produces the deepening of the Aleutian low and the SLP trend pattern over the tropics (negative values in the eastern Pacific and positive values elsewhere). Both forcing agents contribute to the zonally uniform positive Z500 trend in the tropics, with the contribution from sea surface temperature approximately 3 times larger than that from atmospheric radiative forcing. Sea surface temperature trends also lead to a ridge response over the Pacific sector of the high-latitude Southern Ocean.

The distinctive patterns of atmospheric circulation response due to sea surface temperature forcing and direct atmospheric radiative forcing contribute about equally to the global pattern of circulation trends in the SST+ATM simulation, and by inference, nature. The pattern correlations between the SLP (Z500) trends in the SST+ATM ensemble mean and those in the SST and ATM ensemble means are 0.54 and 0.52 (0.75 and 0.44), respectively. In addition to producing distinctive circulation trend responses, sea surface temperature forcing and direct atmospheric radiative forcing also partially offset one another in certain regions: for example, the central North Pacific, tropical eastern Pacific (SLP only), pan-Atlantic, and Southern Ocean.

Figure 5 summarizes the impacts of sea surface temperature forcing and direct atmospheric radiative forcing

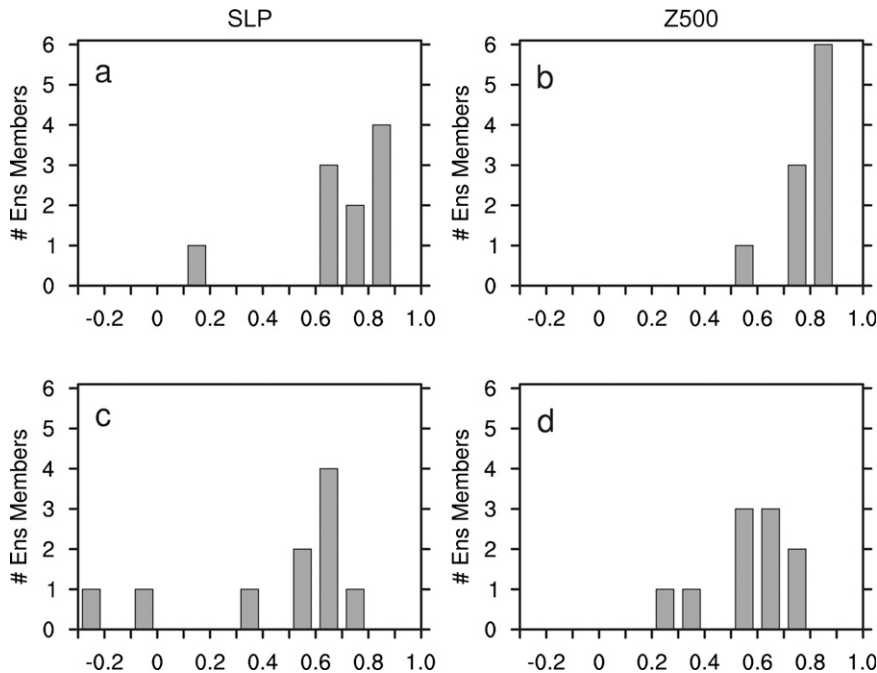


FIG. 4. Histograms of the pattern correlations of DJF trends during 1950–2000 between each individual ensemble member and the ensemble mean from CAM3 SST+ATM experiments for (a) SLP and (b) Z500, and between each individual ensemble member from CAM3 SST+ATM and observations north of 40°S for (c) SLP and (d) Z500.

upon four regional circulation patterns: the Aleutian low, the NAO, the SAM, and the Southern Oscillation. The simulated trends from observations and the model ensemble means (labeled according to their forcing characteristics) are denoted by vertical bars, with dark shading indicating trends that are significant at the 95% confidence level; the trends from the individual ensemble members are denoted by plus signs. The regional circulation patterns are defined as follows. The Aleutian low is given by the “North Pacific index” (NPI; Trenberth and Hurrell 1994), which is the average SLP over the domain (30°–65°N, 160°E–140°W); the NAO is the SLP difference between (55°–90°N, 40°W–65°E) and (30°–55°N, 40°W–65°E); the SAM is the difference in normalized zonally averaged SLP between the latitude bands 37°–47°S and 65°–71°S; and the Southern Oscillation index (SOI) is the SLP difference between the eastern tropical Pacific (20°S–0°, 160°–80°W) and western tropical Pacific (20°S–0°, 80°E–180°) and is used as a proxy for the strength of the Walker circulation.

The observed NPI trend [$-2.6 \text{ hPa (51 yr)}^{-1}$] is well reproduced by the SST+ATM ensemble mean [$-2.2 \text{ hPa (51 yr)}^{-1}$], and both are statistically significant at the 95% level (Fig. 5a). Three of the ensemble members exhibit near-zero trends, while the remaining 7 exhibit trends between -2 and $-4 \text{ hPa (51 yr)}^{-1}$. The

statistically significant NPI trend in the SST ensemble mean [$-3.9 \text{ hPa (51 yr)}^{-1}$] is partially offset by the trend in the ATM ensemble mean [$0.7 \text{ hPa (51 yr)}^{-1}$; not significant], and there is no overlap between any of the individual ensemble members of SST and ATM.

The observed SAM trend [$5.5 \text{ hPa (51 yr)}^{-1}$; note that this is based on station data during 1957–2000, rescaled to units of $(51 \text{ yr})^{-1}$] is also well simulated by the SST+ATM ensemble mean [$3.7 \text{ hPa (51 yr)}^{-1}$], and both are statistically significant at the 95% level. However, there is a sizeable spread among the individual SST+ATM ensemble members, ranging from 1 to 8 hPa (51 yr)^{-1} (Fig. 5c). The statistically significant SAM trend in the ATM ensemble mean [$5.3 \text{ hPa (51 yr)}^{-1}$] is partially offset by the trend in the SST ensemble mean [$-0.9 \text{ hPa (51 yr)}^{-1}$; not significant], with very little overlap between any of the individual ensemble members of SST and ATM.

The results for the NAO and SOI are less robust than those for the NPI and SAM: only the observed NAO trend is statistically significant at the 95% level, while the observed SOI trend and none of the model ensemble mean trends are significant. The observed NAO and SOI trends [4.3 and $-0.65 \text{ hPa (51 yr)}^{-1}$, respectively] are underestimated by the SST+ATM ensemble mean [1.7 and $-0.36 \text{ hPa (51 yr)}^{-1}$, respectively], and there is a large spread among the individual ensemble

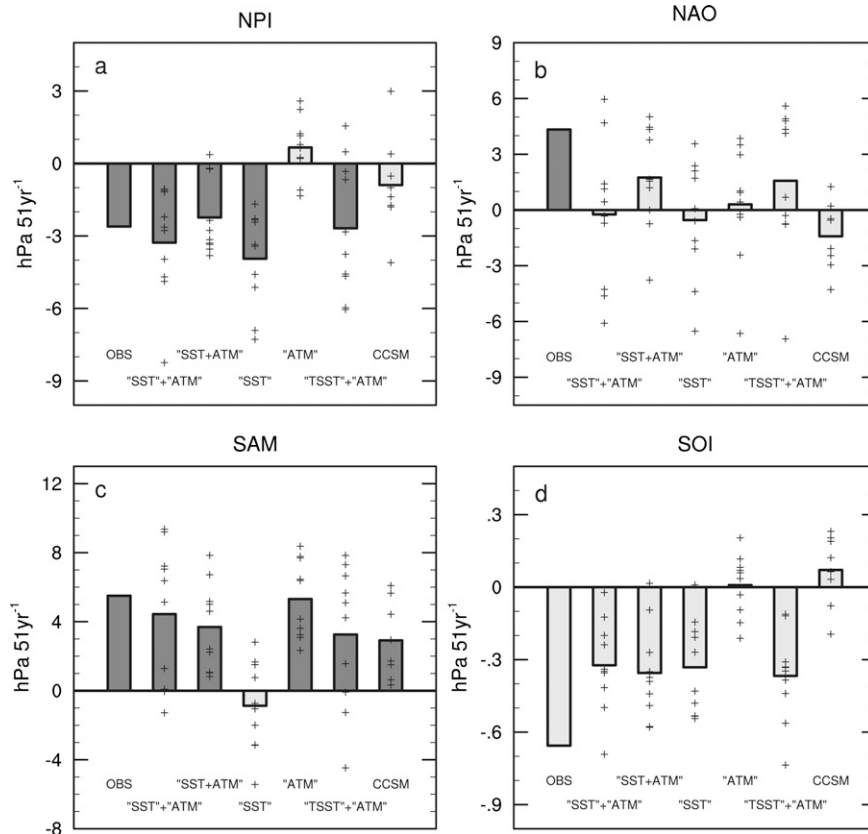


FIG. 5. Regional circulation trends [hPa (51 yr)^{-1}] based on DJF SLP during 1950–2000 for the (a) NPI, (b) NAO, (c) SAM, and (d) SOI from (left to right in each panel) observations (OBS), the sum of CAM3 SST and CAM3 ATM, CAM3 SST + ATM, CAM3 SST, CAM3 ATM, the sum of CAM3 Tropical SST and CAM3 ATM, and CCSM3. For the model simulations, bars denote ensemble mean trends and the plus signs denote individual ensemble member trends. Dark (light) shaded bars indicate trends that are (are not) significantly different from zero at the 95% confidence level.

member trends (Figs. 5b,d). The ATM ensemble mean NAO trend is near zero because of the northward shift of the response relative to that in the SST+ATM ensemble mean (e.g., Fig. 1d versus Fig. 1f), and there is complete overlap between the NAO trends simulated in the individual ensemble members of SST and ATM. The SST ensemble mean SOI trend is nearly identical to that in SST+ATM, while the contribution from the ATM ensemble mean is near zero. Some overlap occurs in the SOI trends between the individual ensemble members of SST and ATM.

c. Linearity of the response to SST and ATM forcing

The degree to which the atmospheric circulation trend responses to sea surface temperature forcing and direct atmospheric radiative forcing are additive may be assessed by comparing the SST+ATM ensemble mean with the sum of the SST and ATM ensemble

means (Fig. 6). Overall, there is a high degree of linearity as evidenced by the similarity of their spatial distributions (pattern correlations of 0.87 and 0.92 for SLP and Z500, respectively) and amplitudes (pattern regressions of 1.06 for both SLP and Z500). Regionally, the amplitudes of the tropical circulation trends are highly linear (see also the SOI in Fig. 5d), while the circulation trends over the North Pacific and extratropical Southern Hemisphere are approximately 20%–30% larger in the sum of the SST and ATM ensemble means than in the SST+ATM ensemble mean (reflected also in the NPI and SAM in Figs. 5a,c). The NAO circulation trends in the SST+ATM ensemble mean are not well reproduced by adding the trends from the SST and ATM ensemble means (see also Fig. 5b).

Another view of the degree of linearity of the atmospheric circulation trend responses to sea surface temperature forcing and direct atmospheric radiative

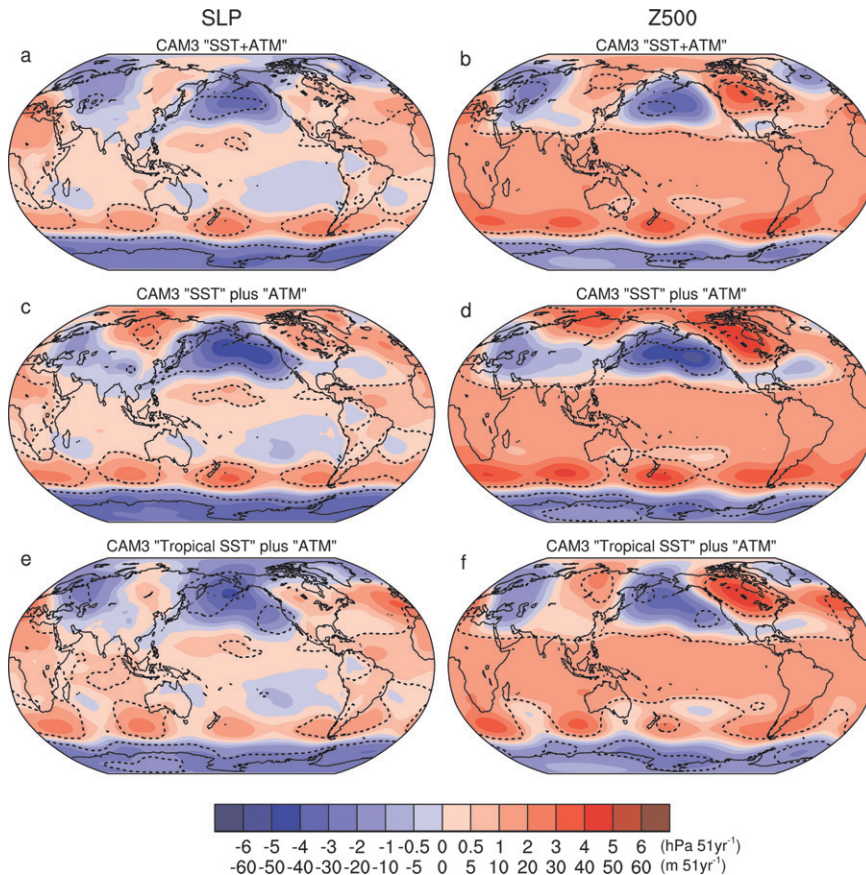


FIG. 6. Linear trends of DJF SLP [left; hPa (51 yr)⁻¹] and Z500 [right; m (51 yr)⁻¹] during 1950–2000 from (a), (b) CAM3 SST+ATM; (c), (d) the sum of CAM3 SST and CAM3 ATM; and (e), (f) the sum of CAM3 Tropical SST and CAM3 ATM. Dashed contours indicate trends that are significantly different from zero at the 95% level.

forcing is given in Fig. 7, which shows the SLP and Z500 trends obtained by subtracting the SST ensemble mean from the SST+ATM ensemble mean. Ostensibly attributable to atmospheric radiative forcing, these trends show similarities and differences with their ATM counterparts (Figs. 1f and 2d). While the SAM and tropical trends are similar to those in the ATM ensemble mean, there are some differences over the extratropical Northern Hemisphere: in particular, the negative trends over the northern center of action of the NAO are considerably larger in magnitude, and the positive trends over the North Pacific are stronger and of greater spatial extent. The extratropical Northern Hemisphere circulation trends obtained using the difference between the SST+ATM and SST experiments exhibit a more zonally symmetric appearance than those obtained from the ATM ensemble directly, especially for Z500. These results are robust for both the T42 and T85 ensemble means individually (not shown).

d. The role of tropical SSTs

The pattern of atmospheric circulation trends simulated by the SST ensemble is reminiscent of that associated with the warm phase of ENSO (not shown but see, e.g., Deser et al. 2006). This suggests that the trend response in the SST ensemble originates from sea surface temperature changes in the tropics. To examine this possibility, we compare the SLP trends simulated by the Tropical SST and SST ensemble means in Fig. 8. There is a high degree of correspondence between the two trend distributions, with a pattern correlation (regression) coefficient of 0.85 (0.83). Similar results are found for the Z500 trends (not shown). It is noteworthy that the extratropical SLP trends, in particular the statistically significant trends over the North Pacific and Southern Ocean, are very similar between the two sets of experiments, indicating that they originate from the tropical portion of the sea surface temperature forcing. The main discrepancy between the SLP trend responses

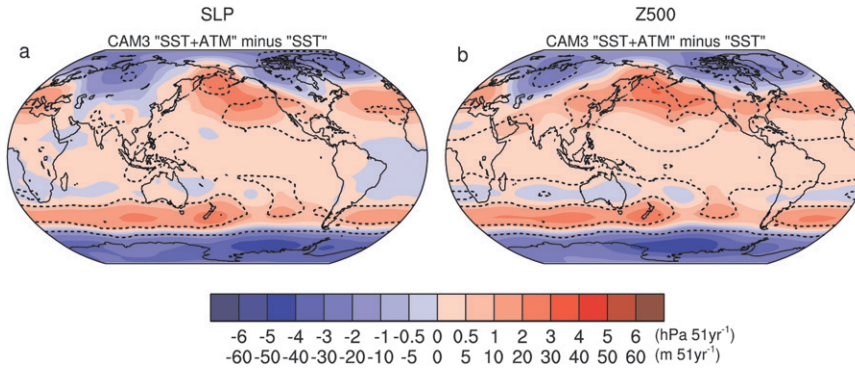


FIG. 7. Linear trends of DJF (a) SLP [$\text{hPa} (51 \text{ yr})^{-1}$] and (b) Z500 [$\text{m} (51 \text{ yr})^{-1}$] during 1950–2000, obtained by subtracting the CAM3 SST ensemble mean from the CAM3 SST+ATM ensemble mean. Dashed contours indicate trends that are significantly different from zero at the 95% level.

to global versus tropical sea surface temperature changes occurs over the North Atlantic, Arctic, and Siberia (e.g., the NAO region) where the responses are opposite in sign, although neither is statistically significant. The tropical control of sea surface temperature-induced global atmospheric circulation trends has been previously highlighted by Schneider et al. (2003), Schubert et al. (2004), and Huang et al. (2005), among others.

The basic mechanism by which tropical sea surface temperature variations impact the extratropical atmo-

spheric circulation is through the meridional dispersion of planetary Rossby waves forced by latent heat release in tropical precipitation, along with attendant feedbacks between the mean flow anomalies and transient eddy activity in midlatitudes (e.g., Hoskins and Karoly 1981; Trenberth et al. 1998). The tropical precipitation trends simulated by the SST and Tropical SST ensemble means show nearly identical patterns, with positive values along the equatorial Pacific and negative values directly to the north as well as over the north-eastern portion of South America (Fig. 8). Except for

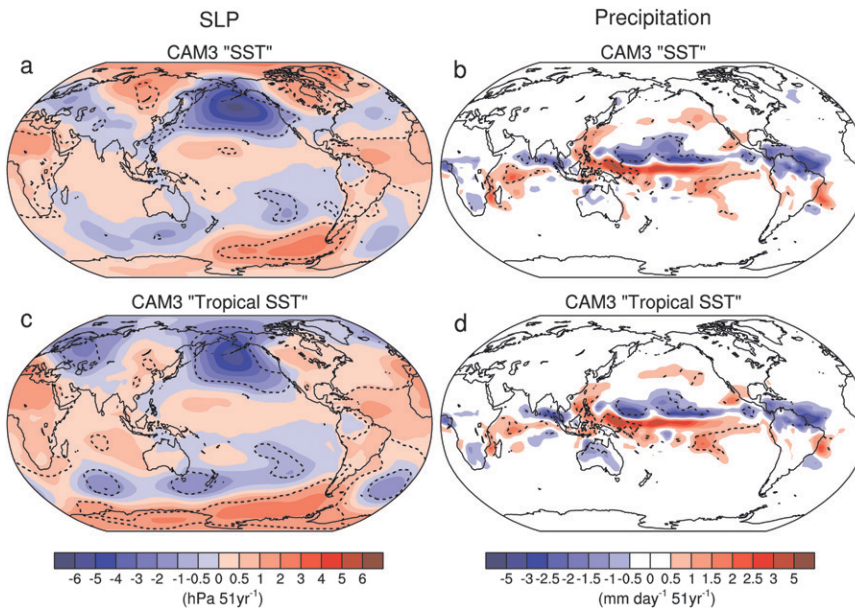


FIG. 8. Linear trends of DJF (left) SLP [$\text{hPa} (51 \text{ yr})^{-1}$] and (right) precipitation [$\text{mm day}^{-1} (51 \text{ yr})^{-1}$] during 1950–2000 from (top) CAM3 SST and (bottom) CAM3 Tropical SST. Dashed contours indicate trends that are significantly different from zero at the 95% level.

the reduced magnitudes within the southern Pacific convergence zone (SPCZ), the simulated precipitation trends resemble those in nature as inferred from trends in marine cloudiness and surface wind convergence (Deser and Phillips 2006) and also those that occur in association with the warm phase of ENSO (Deser et al. 2006). Although not apparent from Fig. 8 because of the color scheme used, the SST and Tropical SST ensembles also reproduce the observed pattern of precipitation trends over North and South America (see, e.g., Deser et al. 2004), consistent with the results of Huang et al. (2005).

Given the similarity between the circulation responses in the SST and Tropical SST ensembles as well as the high degree of linearity of the responses to oceanic and atmospheric radiative forcing, it follows that the circulation trend in the SST+ATM ensemble mean may be reconstructed from the sum of the individual circulation trend responses in the Tropical SST and ATM ensemble means, with pattern correlations of 0.89 for SLP and 0.91 for Z500 (Figs. 6e,f). The goodness of fit of this reconstruction also holds for the regional circulation indices (Fig. 5).

e. Coupled model experiments (CCSM3)

It is of interest to examine the atmospheric circulation trends simulated by CCSM3 and compare them with those from the CAM3 SST+ATM ensemble, given that both sets of model integrations are forced with identical atmospheric radiative changes. We focus on the CCSM3 ensemble mean to isolate primarily the anthropogenically forced component of the simulated trend (recall that the contributions of solar and volcanic forcing are small compared to those of greenhouse gases, ozone, and sulfate aerosols over the second half of the twentieth century; Meehl et al. 2003). Thus, any discrepancies in the atmospheric circulation trends between the CCSM3 ensemble mean and CAM3 SST+ATM (and by inference, nature) are due to differences in their SST evolutions, either as a result of natural (internal) variability in the real climate system, deficiencies in CCSM3's sea surface temperature response to atmospheric radiative forcing, residual internal variability in the 7-member CCSM3 ensemble mean, or a combination of the above.

The SLP and Z500 trends from the CCSM3 ensemble mean exhibit similarities and differences with their CAM3 SST+ATM ensemble mean counterparts (Fig. 9). Similarities include statistically significant trends over the Southern Hemisphere extratropics (negative values over high latitudes coupled with positive values

over midlatitudes, indicative of a positive trend in the SAM; see also Fig. 5c) and statistically significant Z500 trends in the tropics reflecting a warming of the lower troposphere as indicated by an increase in 500–1000-hPa geopotential thickness (not shown). The most notable discrepancies are the SLP trends over the tropical eastern Pacific and Atlantic and the SLP and Z500 trends over the North Atlantic–Eurasian sector, which are of opposite sign in the two models. As a result, the SOI and NAO trends in CCSM3 are of opposite polarity to those in CAM3 (and nature), although neither is statistically significant (Fig. 5). In addition, the deepening of the Aleutian low is about a factor of 3 weaker and not statistically significant in CCSM3 compared to CAM3 (see also Fig. 5a). Overall, the pattern correlation between the ensemble mean CCSM3 and CAM3 SST+ATM trends is 0.47 for SLP and 0.64 for Z500. The pattern correlation between the CCSM3 ensemble mean and observations is 0.19 for SLP and 0.37 for Z500 based on data north of 40°S; considerably weaker than that between the CAM3 SST+ATM ensemble mean and observations (0.73 for SLP and 0.76 for Z500).

Given that both sets of model integrations (CCSM3 and CAM3 SST+ATM) are driven with identical atmospheric radiative forcings, differences in their SST trends are likely responsible for the regional discrepancies in their circulation trends. Indeed, the regions where the two model simulations differ are all areas where SST forcing, and in particular tropical sea surface temperature forcing, is responsible for the circulation trends in CAM3 SST+ATM and by inference nature, with the exception of the North Atlantic–Eurasian sector where the trends are not statistically significant to begin with. Tropical SST trends in CCSM3 are more spatially uniform and weaker in amplitude than in nature, with an average magnitude of $0.3^{\circ}\text{--}0.4^{\circ}\text{C} (51 \text{ yr})^{-1}$ in the model compared to $\sim 0.8^{\circ}\text{C} (51 \text{ yr})^{-1}$ in the tropical Indian and Atlantic and $\sim 1.2^{\circ}\text{C} (51 \text{ yr})^{-1}$ in the eastern Pacific in the observations (Figs. 9e,f). The associated trends in tropical precipitation are considerably smaller in magnitude in CCSM3 compared to those in CAM3 (Figs. 9g,h), which may account for the weaker NPI and SOI trends in the coupled model compared to CAM3 and nature. We have verified that the weak tropical precipitation response in CCSM3 is indeed due to the model's tropical SST simulation: forcing CAM3 with the time-evolving tropical sea surface temperatures from the CCSM3 ensemble mean results in a tropical precipitation trend that is very similar in both amplitude and spatial distribution to that in CCSM3 (not shown).

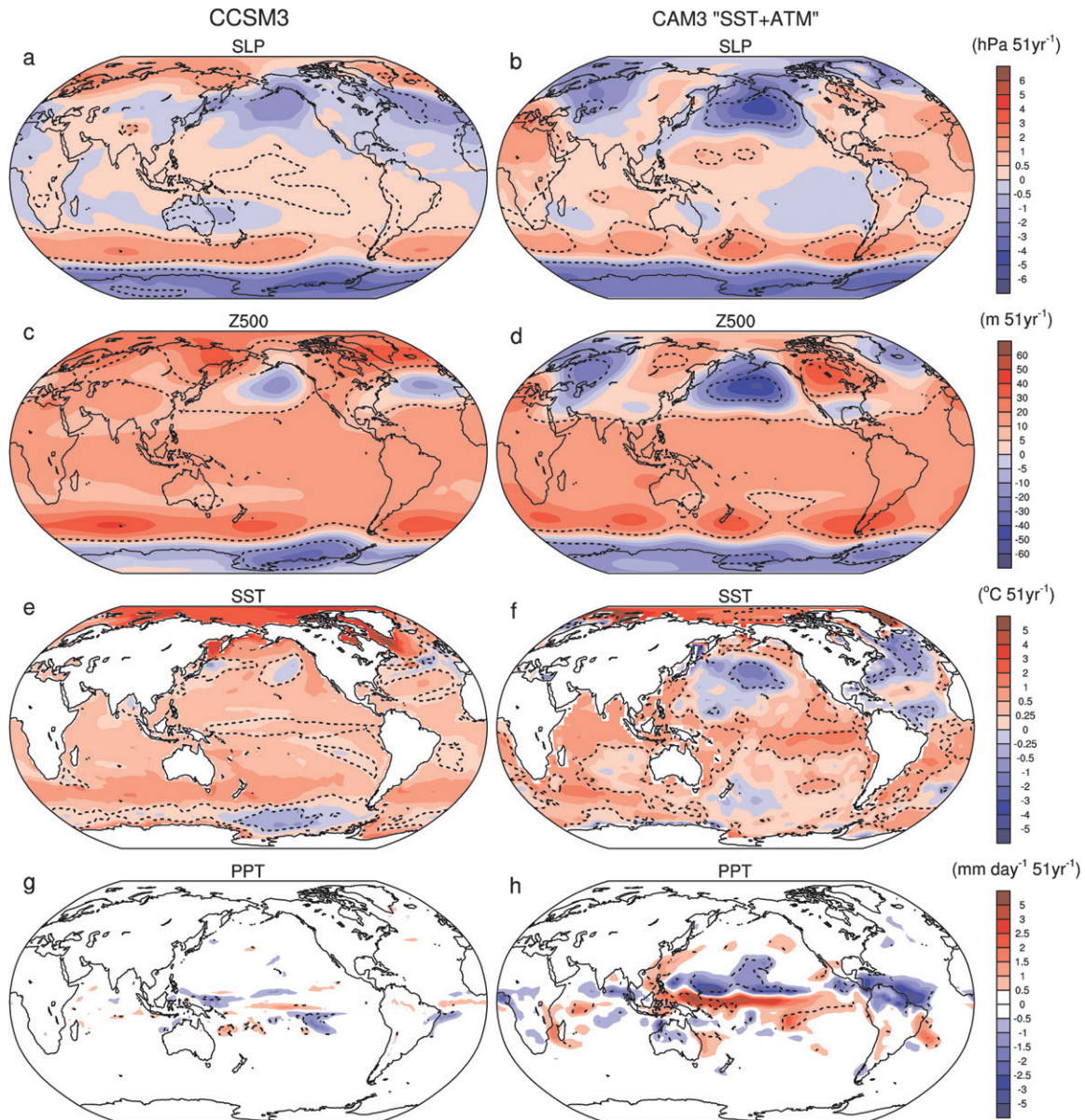


FIG. 9. Linear trends during 1950–99 of DJF (a), (b) SLP [$\text{hPa} (51 \text{ yr})^{-1}$]; (c), (d) Z500 [$\text{m} (51 \text{ yr})^{-1}$]; (e), (f) sea surface temperature [$^{\circ}\text{C} (51 \text{ yr})^{-1}$]; and (g), (h) precipitation [$\text{mm day}^{-1} (51 \text{ yr})^{-1}$] from (left) the CCSM3 ensemble mean and (right) the CAM3 SST+ATM ensemble mean. Color scales are shown to the right; dashed contours indicate trends that are significantly different from zero at the 95% level. Note that sea surface temperature trends in regions of sea ice cover in the Arctic are actually surface temperature trends.

4. Summary and discussion

We have investigated the relative roles of observed sea surface temperature forcing and direct atmospheric radiative forcing (due to observed changes in well-mixed greenhouse gases, tropospheric and stratospheric ozone, sulfate and volcanic aerosols, and solar output) of global DJF atmospheric circulation trends over the second half of the twentieth century by means of ensemble simulations with CAM3, a state-of-the-art

AGCM. The model's 10-member ensemble mean simulates well the observed patterns of SLP and Z500 trends over the globe when forced with the observed evolution of sea surface temperature and atmospheric radiative forcings combined, lending credence to our approach. Individually, sea surface temperature forcing and direct atmospheric radiative forcing produce distinctive circulation responses that contribute about equally to the global pattern of circulation trends. These distinctive circulation responses are approximately additive and

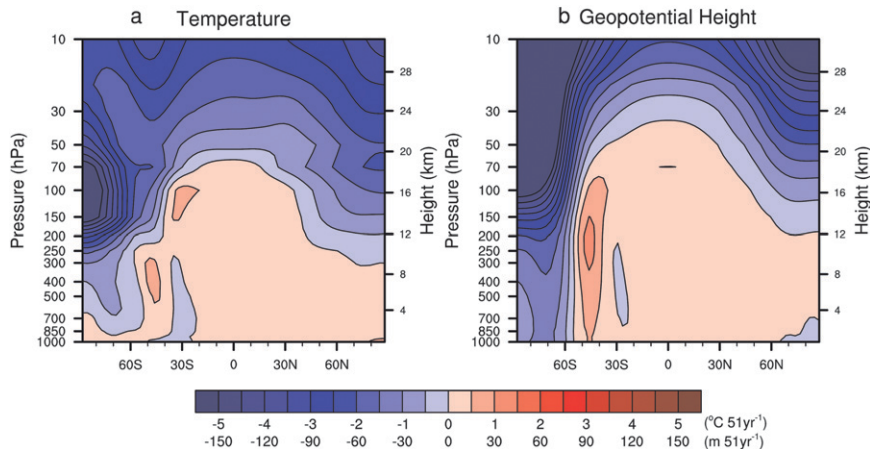


FIG. 10. Linear trends during 1950–2000 of DJF zonally averaged (left) temperature and (right) geopotential height as a function of latitude and pressure from the CAM3 ATM ensemble mean.

partially offsetting. In particular, atmospheric radiative changes directly drive the strengthening and poleward shift of the midlatitude westerly winds in the Southern Hemisphere, manifest as a positive trend in the SAM, and to a lesser extent may contribute to the corresponding feature in the Northern Hemisphere (e.g., a positive trend in the NAO albeit with a northward shift). On the other hand, sea surface temperature changes (specifically those in the tropics) are responsible for the intensification of the Aleutian low and weakening of the tropical Walker circulation. Our findings are generally consistent with those of previous studies, and provide additional insight by clarifying the individual roles of sea surface temperature forcing and direct atmospheric radiative forcing and by placing the regional circulation trends into a global context.

The positive trend in the SAM in recent decades has been attributed to increasing greenhouse gas concentrations and stratospheric ozone depletion in coupled ocean–atmosphere modeling studies (Arblaster and Meehl 2006; Cai and Cowan 2007). Approximately 50%–70% of the SAM trend in Southern Hemisphere summer (DJF) is estimated to be due to ozone depletion, with increases in greenhouse gases being of lesser importance (Arblaster and Meehl 2006; Cai and Cowan 2007). These and other coupled modeling studies do not distinguish between the direct impact of atmospheric radiative forcing and the indirect effect due to altered sea surface temperatures upon the trend in the SAM. In this study, we have shown explicitly that the direct effect of atmospheric radiative forcing is responsible for the positive trend in the SAM during the second half of the twentieth century, with sea surface temperature forcing counteracting this trend (extratropical sea surface tem-

perature forcing acts as a weak positive feedback, but it is overwhelmed by the negative feedback due to tropical sea surface temperature forcing; not shown).

The impact of direct atmospheric radiative forcing on the SAM can be understood from the structure of the zonally averaged temperature trends in the ATM ensemble mean (Fig. 10a). The troposphere exhibits a weak warming trend [$<0.5^{\circ}\text{C} (51 \text{ yr})^{-1}$] north of 60°S while the stratosphere exhibits a strong cooling trend at all latitudes, with amplitudes $\sim -2.5^{\circ}\text{C} (51 \text{ yr})^{-1}$ near 10 hPa and maximum values of $-5.5^{\circ}\text{C} (51 \text{ yr})^{-1}$ at 100 hPa over the South Pole. Note that the stratospheric cooling is stronger and extends to lower altitudes over the South Pole compared to the North Pole. The tropospheric warming and stratospheric cooling are largely a radiative response to greenhouse gas increases, with the enhanced cooling of the lower stratosphere at high latitudes of the Southern Hemisphere radiatively induced by ozone depletion (Randel and Wu 1999; Langematz et al. 2003; Shine et al. 2003). These radiatively induced temperature trends give rise to circulation changes via thermal wind balance, manifest as positive height trends in the troposphere and negative height trends in the stratosphere: the latter extend to the surface south of 60°S (Fig. 10b). A similar downward extension of negative stratospheric height trends to the surface over the southern polar cap since 1979 was shown to be a consequence of stratospheric ozone depletion by Thompson and Solomon (2002, 2005). The lack of a Northern Hemisphere counterpart of this feature may be due in part to the smaller ozone depletion over the North Pole compared to the South Pole (Solomon et al. 2007) coupled with a lack of sunlight in boreal winter.

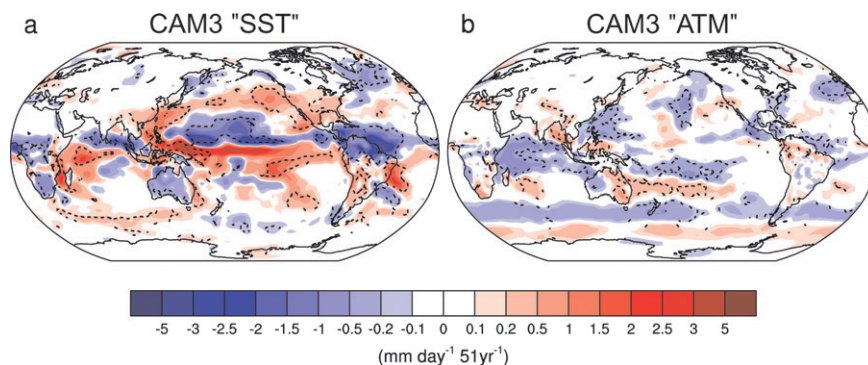


FIG. 11. Linear trends during 1950–2000 of DJF precipitation [$\text{mm day}^{-1} (51 \text{ yr})^{-1}$] from (a) CAM3 SST ensemble mean and (b) CAM3 ATM ensemble mean. Dashed contours indicate trends that are significantly different from zero at the 95% level.

There is a lack of consensus regarding the origin of the positive trend in the NAO. Coupled ocean–atmosphere models (but not CCSM3) collectively indicate a weak upward trend due to atmospheric radiative forcing (direct and indirect), although this trend is not statistically significant compared to the models' internal variability (Gillett et al. 2005); while atmospheric GCMs forced with observed sea surface temperatures yield mixed results, with some indicating a small upward trend due to SST changes in the tropical Indian Ocean (Hoerling et al. 2004; Hurrell et al. 2004) or North Atlantic (Rodwell et al. 1999; Mehta et al. 2000), and others finding no significant oceanic impact but a dominant role for intrinsic atmospheric variability (Schneider et al. 2003; Bracco et al. 2004). None of the NAO trends in the CAM3 ensemble means are statistically significant, and all exhibit large spread among the individual ensemble members as well as nonlinear behavior with respect to the contributions of sea surface temperature and direct atmospheric radiative forcing. Direct atmospheric radiative forcing may play a role, but the centers of action of the NAO-like response are northward shifted with respect to the canonical pattern, precluding a more definitive statement. Thus, the CAM3 results regarding the origin of the positive trend in the NAO remain inconclusive.

The atmospheric circulation responses to sea surface temperature and direct atmospheric radiative forcing tend to be partially offsetting. To explore the origin of this tendency, we compare the tropical precipitation trends in the SST and ATM ensemble means (Fig. 11). Atmospheric radiative forcing produces a general drying trend over the tropical oceans, particularly over the western Indian and Atlantic Oceans, South China Sea, and SPCZ. This drying trend is consistent with the stabilizing influence of atmospheric radiative forcing upon tropospheric lapse rates, which would inhibit deep con-

vection. The general decrease in tropical precipitation due to atmospheric radiative forcing partially counteracts the increase due to sea surface temperature forcing, although there are differences in the spatial patterns of the two rainfall trends (Fig. 11). The radiatively induced tropical drying trend may contribute to the weak positive SLP trends over the North Pacific and eastern tropical Pacific in the ATM ensemble (recall Fig. 1f), providing a mechanism for the partial opposition of sea surface temperature and atmospheric radiative forcing upon the NPI and SOI. Additional experiments using the tropical atmospheric heating response from CAM3 ATM to force CAM3 are needed to fully test this idea.

The counteracting impacts of sea surface temperature and atmospheric radiative changes upon the SAM may also derive from the sea surface temperature-induced tropical precipitation trends. In particular, previous work has shown that tropical precipitation anomalies associated with the warm phase of ENSO force a negative SAM index via changes in the refractivity and rate of dissipation of equatorward-propagating transient waves (Chang 1995; Hou and Molod 1995; Robinson 2002; Seager et al. 2003; L'Heureux and Thompson 2006). The same mechanism may apply to the impact of tropical precipitation trends upon the SAM in the SST ensemble, given that they resemble those during the warm phase of ENSO (recall Fig. 8). We interpret the drying (wetting) trend over the southern ocean mid- (high) latitudes in the ATM ensemble to be a result of the SAM-related circulation changes, not a cause.

With our experimental design, we are unable to address the relative contributions of natural and anthropogenic forcing of observed atmospheric circulation trends during the second half of the twentieth century. However, comparison of the trends simulated by

CAM3 and CCSM3, a fully coupled ocean–atmosphere GCM driven by the identical atmospheric radiative forcings as CAM3, may shed some light upon this issue. Recall that the CCSM3 ensemble mean reflects primarily the coupled model’s response to the anthropogenic component of atmospheric radiative forcing since internally generated variability will be reduced upon averaging across all 7 ensemble members. The amplitude of CCSM3’s ensemble mean tropical Indo-Pacific sea surface temperature warming trend was shown to be ~30% of observed, and the structure is more spatially uniform than that in nature. As a result, the tropical precipitation trend response is considerably weaker in the CCSM3 ensemble mean compared to the CAM3 SST+ATM ensemble mean, which in turn may explain the diminished amplitudes of the SOI and NPI trend responses in CCSM3 compared to CAM3 (and nature).

One possible interpretation of these results is that the portion of the observed tropical Indo-Pacific SST warming trend in excess of the simulated warming trend in the CCSM3 ensemble mean is due to natural (unforced) variability, assuming that the CCSM3 ensemble mean accurately portrays the tropical sea surface temperature response to atmospheric radiative forcing. Taking this interpretation a step further, one may infer that the tropical precipitation trends simulated in CAM3 SST+ATM result almost entirely from the natural component of the observed tropical sea surface temperature trends since the tropical rainfall response to the forced SST trends in CCSM3 is negligible (recall Fig. 9). This line of reasoning suggests that atmospheric teleconnection patterns forced by tropical sea surface temperature changes are also due to natural variability: in particular, the negative trend in the SOI indicative of a weakening of the tropical Walker circulation, and the deepening of the Aleutian low (recall Fig. 8c). Additional support for these conjectures comes from century-long records of tropical Indo-Pacific climate indices and the NPI, which show evidence for coherent multidecadal cycles throughout the twentieth century of which the apparent trend since 1950 is a part (Minobe 1997; Zhang et al. 1997; Deser et al. 2004).

Another valid interpretation is that CCSM3 is deficient in its tropical sea surface temperature and precipitation responses to atmospheric radiative forcing. However, tropical Indo-Pacific sea surface temperature and precipitation trends of similar magnitude to those in the CCSM3 ensemble mean are found in a multimodel ensemble mean derived from 10 different coupled ocean–atmosphere GCMs (excluding CCSM3) from the Third Coupled Model Intercomparison Project (CMIP3) of the World Climate Research Program (and

like CCSM3, the multimodel ensemble mean exhibits negligible Aleutian low and Southern Oscillation responses; not shown). Note that each coupled model was forced with the observed history of atmospheric radiative changes, similar to the CCSM3 simulations. Meehl et al. (2009) also conclude that both natural variability and anthropogenic forcing have contributed to the observed tropical Pacific sea surface temperature trends during the second half of the twentieth century based on a comparison of forced and unforced coupled model simulations. Although these results are suggestive, additional evidence is needed to clarify the relative roles of natural and anthropogenic forcing of observed tropical sea surface temperature and precipitation trends since 1950.

The results of this study highlight the importance of both sea surface temperature and atmospheric radiative changes in forcing global atmospheric circulation trends during 1950–2000. Accurate simulation of both the atmospheric and oceanic responses to increasing greenhouse gases is thus crucial for accurate projections of future atmospheric circulation changes. In addition, the ongoing role of natural sea surface temperature variability must be taken into account when assessing future climate projections.

Acknowledgments. We thank Drs. Grant Branstator, Jian Lu, Jerry Meehl, and Ed Schneider for helpful discussions during the course of this study, and Drs. Mike Alexander, Jim Hurrell, and the anonymous reviewers for their constructive reviews of the manuscript. We thank Drs. Shang-Ping Xie and Yan Du for supplying the CMIP3 output. The authors gratefully acknowledge support from the NOAA CLIVAR program.

REFERENCES

- Allan, R., and T. Ansell, 2006: A new globally complete monthly historical gridded mean sea level pressure dataset (Had-SLP2): 1850–2004. *J. Climate*, **19**, 5816–5842.
- Arblaster, J. M., and G. A. Meehl, 2006: Contributions of external forcing to southern annular mode trends. *J. Climate*, **19**, 2896–2905.
- Bracco, A., F. Kucharski, R. Kallummal, and F. Molteni, 2004: Internal variability, external forcing and climate trends in multi-decadal AGCM ensembles. *Climate Dyn.*, **23**, 659–678.
- Bretherton, C. S., and D. S. Battisti, 2000: An interpretation of the results from atmospheric GCMs forced by the time history of the observed sea surface temperature distribution. *Geophys. Res. Lett.*, **27**, 767–770.
- Cai, W., and T. Cowan, 2007: Trends in Southern Hemisphere circulation in IPCC AR4 models over 1950–99: Ozone depletion versus greenhouse forcing. *J. Climate*, **20**, 681–693.
- Cash, B. A., E. K. Schneider, and L. Bengtsson, 2005: Origin of regional climate differences: Role of boundary conditions and model formulation in two GCMs. *Climate Dyn.*, **25**, 709–723.

- Cayan, D. R., 1992: Latent and sensible heat flux anomalies over the northern oceans: Driving the sea surface temperature. *J. Phys. Oceanogr.*, **22**, 859–881.
- Chang, E. K., 1995: The influence of Hadley circulation intensity changes on extratropical climate in an idealized model. *J. Atmos. Sci.*, **52**, 2006–2024.
- Clarke, A. J., and A. Lebedev, 1996: Long-term changes in the equatorial Pacific trade winds. *J. Climate*, **9**, 1020–1029.
- Collins, W. D., and Coauthors, 2006: The Community Climate System Model Version 3 (CCSM3). *J. Climate*, **19**, 2122–2143.
- Compo, G. P., and P. D. Sardeshmukh, 2008: Oceanic influences on recent continental warming. *Climate Dyn.*, **32**, 333–342.
- Deser, C., and M. S. Timlin, 1997: Atmosphere–ocean interaction on weekly time scales in the North Atlantic and Pacific. *J. Climate*, **10**, 393–408.
- , and A. S. Phillips, 2006: Simulation of the 1976/77 climate transition over the North Pacific: Sensitivity to tropical forcing. *J. Climate*, **19**, 6170–6180.
- , —, and J. W. Hurrell, 2004: Pacific interdecadal climate variability: Linkages between the tropics and the North Pacific during boreal winter since 1900. *J. Climate*, **17**, 3109–3124.
- , A. Capotondi, R. Saravanan, and A. S. Phillips, 2006: Tropical Pacific and Atlantic climate variability in CCSM3. *J. Climate*, **19**, 2451–2481.
- Folland, C. K., D. M. H. Sexton, D. Karoly, C. Johnson, D. Rowell, and D. Parker, 1998: Influences of anthropogenic and oceanic forcing on recent climate change. *Geophys. Res. Lett.*, **25**, 353–356.
- Fyfe, J. C., G. J. Boer, and G. M. Flato, 1999: The Arctic and Antarctic Oscillations and their projected changes under global warming. *Geophys. Res. Lett.*, **26**, 1601–1604.
- Gates, W. L., and Coauthors, 1999: An overview of the results of the Atmospheric Model Intercomparison Project (AMIP I). *Bull. Amer. Meteor. Soc.*, **80**, 29–55.
- Gillett, N. P., and D. W. J. Thompson, 2003: Simulation of recent southern hemisphere climate change. *Science*, **203**, 273–275.
- , R. J. Allan, and T. J. Ansell, 2005: Detection of external influence on sea level pressure with a multi-model ensemble. *Geophys. Res. Lett.*, **32**, L19714, doi:10.1029/2005GL023640.
- Graham, N. E., 1994: Decadal-scale climate variability in the tropical and North Pacific during the 1970s and 1980s: Observations and model results. *Climate Dyn.*, **10**, 135–162.
- Hack, J. J., J. M. Caron, G. Danabasoglu, K. W. Oleson, C. Bitz, and J. Truesdale, 2006: CCSM-CAM3 climate simulation sensitivity to changes in horizontal resolution. *J. Climate*, **19**, 2267–2289.
- Hegerl, G. C., and J. Kenyon, 2008: Influence of modes of climate variability on global temperature extremes. *J. Climate*, **21**, 3872–3889.
- , and Coauthors, 2007: Understanding and attributing climate change. *Climate Change 2007: The Physical Science Basis*, S. Solomon et al., Eds., Cambridge University Press, 663–745.
- Hines, K. M., D. H. Bromwich, and G. J. Marshall, 2000: Artificial surface pressure trends in the NCEP–NCAR reanalyses over the Southern Ocean and Antarctica. *J. Climate*, **13**, 3940–3952.
- Hoerling, M. P., J. W. Hurrell, T. Xu, G. T. Bates, and A. S. Phillips, 2004: Twentieth century North Atlantic climate change. Part II: Understanding the effect of Indian Ocean warming. *Climate Dyn.*, **23**, 391–405.
- Hoskins, B. J., and D. J. Karoly, 1981: The steady linear response of a spherical atmosphere to thermal and orographic forcing. *J. Atmos. Sci.*, **38**, 1179–1196.
- Hou, A. Y., and A. Molod, 1995: Modulation of dynamic heating in the winter extratropics associated with the cross-equatorial Hadley circulation. *J. Atmos. Sci.*, **52**, 2609–2626.
- Huang, H.-P., R. Seager, and Y. Kushnir, 2005: The 1976/77 transition in precipitation over the Americas and the influence of tropical sea surface temperature. *Climate Dyn.*, **24**, 721–740.
- Hurrell, J. W., 1995: Decadal trends in the North Atlantic Oscillation and relationships to regional temperature and precipitation. *Science*, **269**, 676–679.
- , 1996: Influence of variations in extratropical wintertime teleconnections on Northern Hemisphere temperature. *Geophys. Res. Lett.*, **23**, 665–668.
- , and H. van Loon, 1997: Decadal variations associated with the North Atlantic Oscillation. *Climate Change*, **36**, 301–326.
- , M. P. Hoerling, A. S. Phillips, and T. Xu, 2004: Twentieth century North Atlantic climate change. Part I: Assessing determinism. *Climate Dyn.*, **23**, 371–389.
- , J. J. Hack, A. S. Phillips, J. Caron, and J. Yin, 2006: The dynamical simulation of the Community Atmosphere Model Version 3 (CAM3). *J. Climate*, **19**, 2162–2183.
- , —, D. Shea, J. M. Caron, and J. Rosinski, 2008: A new sea surface temperature and sea ice boundary dataset for the Community Atmosphere Model. *J. Climate*, **21**, 5145–5153.
- Kalnay, E., and Coauthors, 1996: The NCEP/NCAR 40-Year Reanalysis Project. *Bull. Amer. Meteor. Soc.*, **77**, 437–471.
- Kistler R., and Coauthors, 2001: The NCEP–NCAR 50-Year Reanalysis: Monthly means CD-ROM and documentation. *Bull. Amer. Meteor. Soc.*, **82**, 247–267.
- Klein, S. A., B. J. Soden, and N.-C. Lau, 1999: Remote sea surface temperature variations during ENSO: Evidence for a tropical atmospheric bridge. *J. Climate*, **12**, 917–932.
- Kumar, A., and M. P. Hoerling, 1998: On the specification of regional SSTs in AGCM simulations. *J. Geophys. Res.*, **103**, 8901–8907.
- Kushner, P. J., I. M. Held, and T. L. Delworth, 2001: Southern Hemisphere atmospheric circulation response to global warming. *J. Climate*, **14**, 2238–2249.
- Langematz, U., M. Kunze, K. Krger, K. Labitzke, and G. L. Roff, 2003: Thermal and dynamical changes of the stratosphere since 1979 and their link to ozone and CO₂ changes. *J. Geophys. Res.*, **108**, 4027, doi:10.1029/2002JD002069.
- L’Heureux, M. L., and D. W. J. Thompson, 2006: Observed relationships between the El Niño–Southern Oscillation and the extratropical zonal-mean circulation. *J. Climate*, **19**, 276–287.
- Marshall, G. J., 2003: Trends in the southern annular mode from observations and reanalyses. *J. Climate*, **16**, 4134–4143.
- Meehl, G. A., W. M. Washington, T. M. L. Wigley, J. M. Arblaster, and A. Dai, 2003: Solar and greenhouse gas forcing and climate response in the twentieth century. *J. Climate*, **16**, 426–444.
- , and Coauthors, 2006: Climate change projections for the twenty-first century and climate change commitment in the CCSM3. *J. Climate*, **19**, 2597–2616.
- , A. Hu, and B. Santer, 2009: The mid-1970s climate shift in the Pacific and the relative roles of forced versus inherent decadal variability. *J. Climate*, **22**, 814–826.
- Mehta, V., M. Suarez, J. V. Manganello, and T. D. Delworth, 2000: Oceanic influence on the North Atlantic Oscillation and associated Northern Hemisphere climate variations: 1959–1993. *Geophys. Res. Lett.*, **27**, 121–124.

- Minobe, S., 1997: A 50-70 year climatic oscillation over the North Pacific and North America. *Geophys. Res. Lett.*, **24**, 683–686.
- Power, S. B., and I. N. Smith, 2007: Weakening of the Walker circulation and apparent dominance of El Niño both reach record levels, but has ENSO really changed? *Geophys. Res. Lett.*, **34**, L18702, doi:10.1029/2007GL030854.
- Randel, W. J., and F. Wu, 1999: Cooling of the Arctic and Antarctic polar stratospheres due to ozone depletion. *J. Climate*, **12**, 1467–1479.
- Robinson, W. A., 2002: On the midlatitude thermal response to tropical warmth. *Geophys. Res. Lett.*, **29**, 1190, doi:10.1029/2001GL014158.
- Rodwell, M. J., D. P. Rowell, and C. K. Folland, 1999: Oceanic forcing of the wintertime North Atlantic Oscillation and European climate. *Nature*, **398**, 320–323.
- Schneider, E. K., L. Bengtsson, and Z. Hu, 2003: Forcing of northern hemisphere climate trends. *J. Atmos. Sci.*, **60**, 1504–1521.
- Schubert, S. D., M. J. Suarez, P. J. Pegion, R. D. Koster, and J. T. Bacmeister, 2004: Causes of long-term drought in the U.S. Great Plains. *J. Climate*, **17**, 485–503.
- Seager, R., N. Harnik, Y. Kushnir, W. Robinson, and J. A. Miller, 2003: Mechanisms of hemispherically symmetric climate variability. *J. Climate*, **16**, 2960–2978.
- Shine, K. P., and Coauthors, 2003: A comparison of model-simulated trends in stratospheric temperatures. *Quart. J. Roy. Meteor. Soc.*, **129**, 1565–1588.
- Solomon, S., R. W. Portmann, and D. W. J. Thompson, 2007: Contrasts between Antarctic and Arctic ozone depletion. *Proc. Natl. Acad. Sci. USA*, **104**, 445–449, doi:10.1073/pnas.0604895104.
- Stephenson, D. B., and I. M. Held, 1993: GCM response of northern winter stationary waves and storm tracks to increasing amounts of carbon dioxide. *J. Climate*, **6**, 1859–1870.
- Tanaka, H. L., I. Noriko, and A. Kitoh, 2004: Trend and interannual variability of Walker, monsoon and Hadley circulations defined by velocity potential in the upper troposphere. *Tellus*, **56A**, 250–269, doi:10.1111/j.1600-0870.2004.00049.
- Thompson, D. W. J., and S. Solomon, 2002: Interpretation of recent Southern Hemisphere climate change. *Science*, **296**, 895–899.
- , and —, 2005: Recent stratospheric climate trends: Global structure and tropospheric linkages. *J. Climate*, **18**, 4785–4795.
- , J. M. Wallace, and G. C. Hegerl, 2000: Annular modes in the extratropical circulation. Part II: Trends. *J. Climate*, **13**, 1018–1036.
- Trenberth, K. E., and J. W. Hurrell, 1994: Decadal atmosphere-ocean variations in the Pacific. *Climate Dyn.*, **9**, 303–319.
- , G. W. Branstator, D. Karoly, A. Kumar, N. Lau, and C. Ropelewski, 1998: Progress during TOGA in understanding and modeling global teleconnections associated with tropical sea surface temperatures. *J. Geophys. Res.*, **103**, 14 291–14 324.
- von Storch, H., and F.W. Zwiers, 1999: *Statistical Analysis in Climate Research*. Cambridge University Press, 484 pp.
- Worley, S. J., S. D. Woodruff, R. W. Reynolds, S. J. Lubker, and N. Lott, 2005: ICOADS release 2.1 data and products. *Int. J. Climatol.*, **25**, 823–842.
- Zhang, Y., J. M. Wallace, and D. S. Battisti, 1997: ENSO-like interdecadal variability: 1900–93. *J. Climate*, **10**, 1004–1020.